Available online at www.sciencedirect.com

ScienceDirect

IFAC PapersOnline CONFERENCE PAPER ARCHIVE

IFAC PapersOnLine 55-22 (2022) 212–217

Separate Guidance and Control Design for Autonomous Path-following

Saurabh Kumar *, **Shashi Ranjan Kumar** *, and **Abhinav Sinha** **

* *Intelligent Systems & Control Lab, Department of Aerospace Engineering, Indian Institute of Technology Bombay, Powai- 400076, Mumbai, India*

** *Unmanned Systems Lab, Department of Electrical and Computer Engineering, The University of Texas at San Antonio, San Antonio, Texas 78249, USA*

Abstract: This paper addresses the separate guidance and control design for an unmanned aerial vehicle (UAV) to follow the desired path with arbitrary curvature. The proposed design is appealing since it neither requires the information about the path curvature to be implemented nor necessitates tracking a moving virtual target. Such a feature makes our design simple and elegant. We first show that it is sufficient to nullify the UAV's perpendicular distance with respect to the path in order for it to track and follow the desired path and that there is no restriction on the UAV's initial configuration. This makes the proposed design globally valid. Next, we augment the UAV's guidance system with an autopilot obtained by approximating its higher-order dynamics as a second-order transfer function. We demonstrate the efficacy of the proposed design through simulations for various scenarios.

Keywords: Unmanned Aerial Vehicle (UAV), Path-following, Guidance and Control, Sliding Mode Control.

1. INTRODUCTION

The broad applicability of autonomous vehicles, especially UAVs, necessitates the development of a robust guidance system for motion planning such as path-following, trajectory tracking (Kumar and Kumar, 2022a,b), obstacle avoidance, survival (Kumar S et al., 2022), etc. In this work, we look at a path-following scenario, which is a crucial component of any automated flight control system and has a wide range of applications, including waypoint navigation, following a pre-programmed course, and autonomous landing. In a path-following problem, the objective is to allow the vehicle to converge to and follow the pre-specified path without needing any temporal constraints. This feature makes the design more flexible than trajectory tracking or target capture scenarios that account for spatiotemporal constraints.

In the existing literature, various linear and nonlinear controllers have been proposed for the path-following of a UAV. For example, Yoshitani (2010) presented a proportional-integral-derivative (PID) controller for UAV path-following, whereas Ratnoo et al. (2011) proposed a linear quadratic regulator (LQR) based controller for a UAV to follow the desired path. For the same objective, Rhee et al. (2010) developed a feedforward controller using the cubic spline method by representing the original path using a set of points. Although such techniques were easier to implement, they may not guarantee satisfactory performance when the UAV initially has a large deviation from the desired path or if the path is characterized by complex curvatures. Additionally, those controllers were also susceptible to external disturbances.

In order to overcome the limitations associated with the linear control methods, several nonlinear controllers were also proposed, which can be broadly divided into three sub-categories– the error-regulation approach, the vector-field guidance, and the virtual-target concept. In the first sub-category (e.g., see (Cabecinhas et al., 2007; Gates, 2010; Kaminer et al., 2010; Liu et al., 2012; Yamasaki et al., 2013)), the authors have defined a suitable error variable, such as cross-track error, along-track error, vehicle heading error, etc., and converted the path following problem into the regulation of error dynamics, and then applied nonlinear control methods to regulate these errors. In the second sub-category, a vector field matching the desired course angle or desired velocity was created so that the UAV may converge to the target path along that field (e.g., (Frew et al., 2007; Lawrence et al., 2008; Nelson et al., 2007)). In the third sub-category, the authors have assumed to have a virtual target point on the path. Their guidance laws steer the UAV toward the path by chasing that point. Most of the works in this sub-category were geometric and established on the concept of autonomous guidance (e.g., see the works of Lizarraga et al. (2013); Park et al. (2007); Ratnoo et al. (2015); Singh et al. (2022)).

However, most existing works focused on the guidance aspect only; that is, most existing path-following controllers design only the guidance command for the UAV while neglecting the autopilot dynamics under the premise

10.1016/j.ifacol.2023.03.036

that the inner control loop has no lag. Clearly, such an assumption may not always be valid in practice. In this paper, we propose a separate guidance and control design where we first derive the guidance command providing advantages compared to the existing ones. Additionally, we also augment the guidance system with an autopilot, which effectively generates the command necessary to steer the UAV toward the path. The proposed design remains valid for arbitrary initial configurations of the UAV and does not depend on the path curvature, which is unlike strategies based on vector-field guidance. In other words, our proposed strategy can guarantee that a UAV follows the desired path irrespective of its curvature. Further, the proposed design is based on the concept of global finite-time error convergence and favors easy implementation using inexpensive onboard sensors.

The rest of this paper is organized as follows. First, we discuss the UAV kinematics and state the problem addressed in this paper in Section 2. Furthermore, in Sections 3 and 4, we design the proposed the guidance and autopilot. We demonstrate the robust performance of the proposed technique in Section 5 via numerical simulations, followed by the concluding remarks in Section 6.

2. PROBLEM FORMULATION

Consider a UAV flying at a constant altitude, essentially leading to a planar engagement. The UAV is a non-holonomic vehicle steered by its lateral acceleration, a_m, which is perpendicular to its velocity. We denote the UAV's speed and the heading angle from a reference direction using $v \in \mathbb{R}_+$ and $\psi \in \mathbb{R}$, respectively. For some $[x,\ y]^T \in \mathbb{R}^2$ denoting the position of the UAV, one has

$$\dot{x} = v\cos\psi, \dot{y} = v\sin\psi, \dot{\psi} = \frac{a_m}{v}. \tag{1}$$

Fig. 1 shows a typical scenario wherein the UAV is required to follow the desired path. We assume that the path is smooth, whose curvature is unknown to the UAV's guidance system.

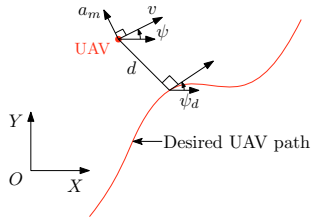

Fig. 1. Illustration of the path-following problem.

From Fig. 1, one may write the perpendicular distance between the UAV and the desired path as d while ψ_d represents the reference path angle. It is apparent that d is finite and bounded. Hence, one may write

$$\dot{d} = v\sin(\psi - \psi_d), \tag{2}$$

which also remains finite and bounded. It is worth noting that $\dot{\psi}_d$ may not be known to the UAV's guidance system as it depends on the desired path curvature information.

To elucidate the idea, we present two special path constructs, namely, a straight-line path (shown in Fig. 2(a)) and a circular orbit (depicted in Fig. 2(b)).

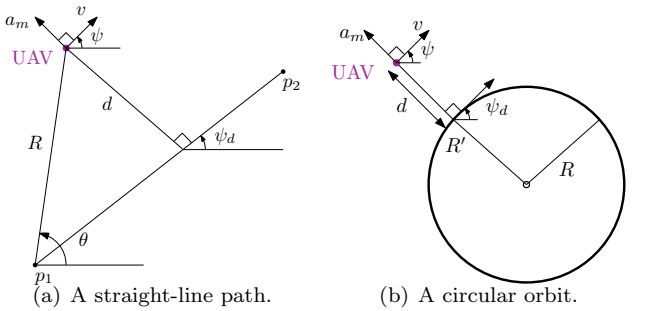

(a) A straight-line path. (b) A circular orbit.

Fig. 2. Special path constructs.

The straight-line path, shown in Fig. 2(a), is formed by joining two points p_1 and p_2. If we assume that the UAV is at a radial distance, R, from p_1 and subtends an angle, θ, from the reference, then one may compute d as

$$d = R\sin(\theta - \psi_d), \tag{3}$$

whose rate of change is the same as (2). Similarly, for a circular orbit of radius, R, and the UAV located at a distance R' from the center of the circle, we have

$$d = R' - R. \tag{4}$$

and corresponding rate of change as (2). One may observe that while the distance d changes depending on the path, $\dot{d}$ remains the same regardless of the path. This indicates that the proposed technique is applicable for a generic path since it only requires d and $\dot{d}$ to vanish in order for the UAV to follow the desired path.

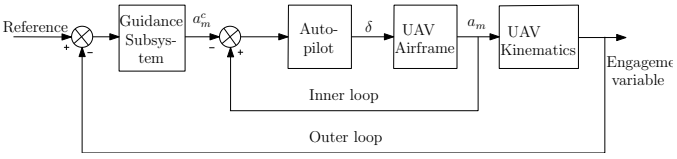

Fig. 3. Schematic diagram of the separate guidance and control design.

From a practical perspective, the overall design should consider both guidance and control aspects since accounting for system lag (the inner loop) leads to a more accurate design than having the outer loop alone. Further, note that autopilot is a higher-order system, typically having thirteenth-order dynamics (Gurfil, 2003). However, it can be approximated as a second-order transfer function (Gurfil, 2003; Gutman, 2008). Such an approximation has also been used to validate the guidance law proposed by Sinha et al. (2021). To this end, we consider a second-order transfer function,

$$\frac{a_m}{\delta} = \frac{\omega_n^2}{s^2 + 2\xi\omega_n s + \omega_n^2}, \tag{5}$$

where δ is the applied lateral acceleration, ω_n is the undamped natural frequency, and ξ represents the damping ratio.

Fig. 3 depicts the schematic representation of the proposed separate guidance and control path-following feedback controller. It consists of two loops: the outer loop and the inner loop. The outer loop, known as the guidance loop, generates the necessary guidance command to nullify the perpendicular distance between the UAV and the desired path. The inner consists of the autopilot, which nullifies

the error between the designed steering command and the demanded one.

This paper aims to separately design nonlinear feedback controllers for the UAV's guidance and the control subsystems such that the UAV converges to the desired path within a finite time and follows the same thereafter. We further require that the design remains globally valid, even when the UAV has large initial deviations from the path.

3. DESIGN OF THE GUIDANCE SUBSYSTEM

The guidance subsystem forms the outer loop. We first design the necessary guidance command, a_m, for the UAV such that it tracks the desired path within a finite time and stays on it thereafter. Because at any time instant, the UAV and the path are separated by a perpendicular distance, d, one may think of d as a metric whose nullification could steer the UAV on the desired path. To this end, we look at the distance d and its rate of change $\dot{d}$ closely before deriving the proposed command.

Differentiating (2) with respect to time yields

$$\ddot{d} = v\cos(\psi-\psi_d)\left(\dot{\psi}-\dot{\psi}_d\right), \tag{6}$$

which can be further simplified, by substituting (1) into (6), to

$$\begin{aligned}\ddot{d} &= v\cos(\psi-\psi_d)\left(\frac{a_m^c}{v}-\dot{\psi}_d\right)\\ &= a_m^c\cos(\psi-\psi_d) - v\dot{\psi}_d\cos(\psi-\psi_d).\end{aligned} \tag{7}$$

In the absence of the path curvature information, the term $\dot{\psi}_d$ can be treated as a bounded uncertainty, that is,

$$\ddot{d} = a_m^c\cos(\psi-\psi_d) + \Delta, \tag{8}$$

where $\Delta = -v\dot{\psi}_d\cos(\psi-\psi_d)$, such that $|\Delta| \le \Delta_{\max} < \infty$.

It follows that the dynamics of the perpendicular separation between the UAV and the desired path has a relative degree of two with respect to the UAV's commanded lateral acceleration, a_m^c.

Thus, the objective of designing a path-following controller can be thought of as designing a suitable a_m^c that stabilizes the above dynamical system, (8). To design the controller, we consider a switching surface given by

$$\mathcal{S}_d = d + \frac{1}{\beta_d}\dot{d}^{p_d/q_d}, \tag{9}$$

where $\beta_d > 0$, p_d, and q_d are odd positive integers such that $p_d > q_d$, and $1 < \frac{p_d}{q_d} < 2$. It is important to note that such choices of p_d and q_d always ensure that one of the roots of $(\cdot)^{p_d/q_d}$ will be real and will also preserve its sign.

It is advantageous for us to use the sliding mode control for the specific problem discussed in this paper since by enforcing sliding mode on the chosen manifold, (9), the UAV can be made to follow the desired path when the controller has no knowledge of exact Δ, but its maximum bound is available to the designer.

On differentiating the switching surface, $\mathcal{S}_d$, with respect to time, one can get

$$\dot{\mathcal{S}}_d = \dot{d} + \frac{1}{\beta_d}\frac{p_d}{q_d}\dot{d}^{p_d/q_d-1}\ddot{d}, \tag{10}$$

which can be written, using (8), as

$$\dot{\mathcal{S}}_d = \dot{d} + \frac{1}{\beta_d}\frac{p_d}{q_d}\dot{d}^{p_d/q_d-1}\left(a_m^c\cos(\psi-\psi_d)+\Delta\right). \tag{11}$$

Now let us consider a radially unbounded Lyapunov candidate as $\mathcal{V}(\mathcal{S}_d) = \frac{1}{2}\mathcal{S}_d^2$. The time derivative of the Lyapunov candidate, $\mathcal{V}$, can be obtained using (11) as

$$\dot{\mathcal{V}} = \mathcal{S}_d\dot{\mathcal{S}}_d = \mathcal{S}_d\left[\dot{d} + \frac{1}{\beta_d}\frac{q_d}{p_d}\dot{d}^{p/q-1}\left(a_m^c\cos(\psi-\psi_d)+\Delta\right)\right].$$

If we design the commanded lateral acceleration as

$$a_m^c = \frac{-1}{\cos(\psi-\psi_d)}\left[\beta\frac{q}{p}\dot{d}^{2-p/q} + \eta\,\mathrm{sign}(\mathcal{S}_d)\right], \tag{12}$$

where $\eta > \Delta_{\max}$, then the derivative of Lyapunov candidate reduces to

$$\begin{aligned}\dot{\mathcal{V}}(d) =& \mathcal{S}_d\left[\dot{d} + \frac{1}{\beta_d}\frac{p_d}{q_d}\dot{d}^{p_d/q_d-1}\left(-\beta_d\frac{q_d}{p_d}\dot{d}^{2-p_d/q_d}\right.\right.\\ &\left.\left.-\eta\,\mathrm{sign}(\mathcal{S}_d)+\Delta\right)\right],\\ =& \mathcal{S}_d\left[\frac{1}{\beta_d}\frac{p_d}{q_d}\dot{d}^{p_d/q_d-1}\left(-\eta\,\mathrm{sign}(\mathcal{S}_d)+\Delta\right)\right],\\ \le& -\frac{1}{\beta_d}\frac{p_d}{q_d}\left(\eta-\Delta_{\max}\right)\dot{d}^{p_d/q_d-1}|\mathcal{S}_d|,\\ \le& -\frac{1}{\beta_d}\frac{p_d}{q_d}\eta\dot{d}^{p_d/q_d-1}|\mathcal{S}_d|,\end{aligned} \tag{13}$$

which implies that $\dot{\mathcal{V}}(d) < 0\ \forall\ \mathcal{S}_d \neq 0$ if $\eta > \Delta_{\max}$, as the terms $\beta_d, p_d, q_d > 0$.

Note that p_d and q_d are odd positive integers such that $1 < p_d/q_d < 2$, we always have $(p_d - q_d)$ as an even integer and $\dot{d}^{p_d/q_d-1} = \dot{d}^{(p_d-q_d)/q_d} > 0\ \forall\ \dot{d} \neq 0$. Let us now define

$$\rho(d) := \frac{1}{\beta_d}\frac{p_d}{q_D}\eta\dot{d}^{p_d/q_d-1}, \tag{14}$$

then $\dot{\mathcal{V}}$ in (13) satisfies

$$\dot{\mathcal{V}} \le \rho(d)|\mathcal{S}_d|. \tag{15}$$

Since, $\rho(d) > 0\ \forall\ \dot{d} \neq 0$, the Lyapunov stability criteria is satisfied $\forall\ \dot{d} \neq 0$, and the errors d, and $\dot{d}$ will subsequently vanish once $\mathcal{S}_d = 0$.

On substituting the guidance command from (12) into (8), we obtain $\ddot{d}$ as

$$\ddot{d} = -\beta_d\frac{p_d}{q_d}\dot{d}^{2-p_d/q_d} - \eta\,\mathrm{sign}(\mathcal{S}_d) + \Delta. \tag{16}$$

For $\dot{d} = 0$, (16) reduces to

$$\ddot{d} = -\eta\,\mathrm{sign}(\mathcal{S}_d) + \Delta. \tag{17}$$

Now, if $\mathcal{S}_d > 0$, then $\ddot{d} \le -\eta$ as $\eta > \Delta_{\max} \ge 0$. Similarly, when $\mathcal{S}_d < 0$, we have $\ddot{d} \ge \eta$. These cases imply that $\dot{d} = 0$ is not an attractor and that there always exists a small neighborhood, $\mathcal{N}(\gamma)$, such that $|\dot{d}| < \gamma$ for any $\gamma > 0$. Consequently, the trajectories will cross the boundaries $\dot{d} = \gamma$ and $\dot{d} = -\gamma$ within a finite time, irrespective of their initial values. In other words, trajectories starting from arbitrary initial conditions are attracted towards the sliding manifold, (9), within a finite time.

When the sliding mode is enforced on $\mathcal{S}$, that is, the trajectories have reached the sliding manifold, then the perpendicular separation between the UAV and the path is governed by reduced-order dynamics,

$$\dot{d} = -\beta_d d^{q_d/p_d}. \tag{18}$$

Solving for a time instant t_1 such that $d = 0 \; \forall \; t > t_1$ for a given initial condition $d(t_0)$ at $t = t_0$, one may obtain

$$\begin{aligned} t_1 &= t_0 - \frac{1}{\beta_d} \int_{d(t_0)}^{0} d^{-q_d/p_d} \, \mathrm{d}(d), \\ &= t_0 + \frac{p_d}{\beta_d (p_d - q_d)} d^{\frac{p_d - q_d}{p_d}} d(t_0). \end{aligned} \tag{19}$$

Note that since $(p_d - q_d)$ is a positive even integer, d converges to zero within a finite time, t_1, and remains there $\forall \; t \geq t_1$, which further implies $\dot{d} = 0$ within the same time. Consequently, the UAV is able to track the desired path within a time instant t_1, given by (19), from arbitrary initial configurations even without the knowledge of the exact path curvature.

4. DESIGN OF THE AUTOPILOT

The control subsystem forms the inner loop. The commanded value of lateral acceleration, which we designed in the previous section, is not instantaneously applied to adjust the UAV's course toward the path. Instead, the commanded acceleration acts an an input to the autopilot whose dynamics is of second order. At each instant, the error between the commanded and the achieved lateral accelerations, say $\mathcal{S}_\varrho$, is used by the autopilot as a correction variable.

Similar to the previous design, we define the error between the commanded and actual guidance command as $\varrho = a_m - a_m^c$, and its rate as $\dot{\varrho} = \dot{a}_m - \dot{a}_m^c$. The dynamics of $\dot{\varrho}$ is expressed as

$$\ddot{\varrho} = \ddot{a}_m - \ddot{a}_m^c = -2\xi\omega_n \dot{a}_m - a_m \omega_n^2 - \ddot{a}_m^c + \omega_n^2 \delta, \tag{20}$$

which implies that the dynamics of ϱ has a relative degree of two with respect to δ.

Our next goal is to nullify the error, ϱ such that as $\varrho \to 0$ within a finite time, $a_m^c \to a_m$ within the same time. Thus, we consider another sliding manifold,

$$\mathcal{S}_\varrho = \varrho + \frac{1}{\beta_\varrho} \dot{\varrho}^{p_\varrho / q_\varrho}, \tag{21}$$

where $\beta_\varrho > 0$, p_ϱ, and q_ϱ are odd positive integers satisfying $p_\varrho > q_\varrho$, and $1 < \dfrac{p_\varrho}{q_\varrho} < 2$. These design parameters are similar to the ones presented in the previous section.

On differentiating the switching manifold, (21), with respect to time, one may obtain

$$\dot{\mathcal{S}}_\varrho = \dot{\varrho} + \frac{p_\varrho}{\beta_\varrho q_\varrho} \dot{\varrho}^{(p_\varrho/q_\varrho - 1)} \ddot{\varrho}. \tag{22}$$

If we substitute for $\ddot{\varrho}$ from (20) in (22), we obtain

$$\begin{aligned} \dot{\mathcal{S}}_\varrho =& \dot{\varrho} + \frac{p_\varrho}{\beta_\varrho q_\varrho} \dot{\varrho}^{(p_\varrho/q_\varrho - 1)} \\ & \times \left[-2\xi\omega_n \dot{a}_m - a_m \omega_n^2 - \ddot{a}_m^c + \omega_n^2 \delta \right]. \end{aligned} \tag{23}$$

Similar to the previous part, we consider another Lyapunov function candidate as $\mathcal{V}(\mathcal{S}_\varrho) = \dfrac{1}{2} \mathcal{S}_\varrho^2$, which is a radially unbounded function such that $\mathcal{V}(\mathcal{S}_\varrho) > 0 \; \forall \; \mathcal{S}_\varrho \neq 0$ and $\mathcal{V}(\mathcal{S}_\varrho) = 0$ only if $\mathcal{S}_\varrho = 0$.

On differentiating the Lyapunov function candidate,$\mathcal{V}(\mathcal{S}_\varrho)$, with respect to time, one may obtain

$$\begin{aligned} \dot{\mathcal{V}}_\varrho =& \mathcal{S}_\varrho \dot{\mathcal{S}}_\varrho \\ =& \mathcal{S}_\varrho \left[\dot{\varrho} + \frac{p_\varrho}{\beta_\varrho q_\varrho} \dot{\varrho}^{(p_\varrho/q_\varrho - 1)} \left(-2\xi\omega_n \dot{a}_m - a_m \omega_n^2 \right. \right. \\ & \left. \left. - \ddot{a}_m^c + \omega_n^2 \delta \right) \right]. \end{aligned} \tag{24}$$

If we design the applied lateral acceleration, δ, as

$$\begin{aligned} \delta = & -\frac{1}{\omega_n^2} \left[-2\xi\omega_n \dot{a}_m - a_m \omega_n^2 - \ddot{a}_m^c + \beta_\varrho \frac{p_\varrho}{q_\varrho} \dot{\varrho}^{2 - p_\varrho/q_\varrho} \right. \\ & \left. + \mathcal{K} \mathrm{sign}(\mathcal{S}_\varrho) \right], \end{aligned} \tag{25}$$

with $\mathcal{K} > 0$, then (24) reduces to

$$\begin{aligned} \dot{\mathcal{V}}_\varrho = \mathcal{S}_\varrho \left[\dot{\varrho} + \frac{p_\varrho}{\beta_\varrho q_\varrho} \dot{\varrho}^{(p_\varrho/q_\varrho - 1)} \left\{ -2\xi\omega_n \dot{a}_m - a_m \omega_n^2 - \ddot{a}_m^c \right. \right. \\ + \omega_n^2 \frac{-1}{\omega_n^2} \left(-2\xi\omega_n \dot{a}_m - a_m \omega_n^2 - \ddot{a}_m^c + \beta_\varrho \frac{p_\varrho}{q_\varrho} \dot{\varrho}^{2 - p_\varrho/q_\varrho} \right. \\ \left. \left. \left. + \mathcal{K} \mathrm{sign}(\mathcal{S}_\varrho) \right) \right\} \right], \end{aligned} \tag{26}$$

which, on simplification, yields

$$\begin{aligned} \dot{\mathcal{V}}_\varrho =& \mathcal{S}_\varrho \left[\dot{\varrho} - \frac{p_\varrho}{\beta_\varrho q_\varrho} \dot{\varrho}^{(p_\varrho/q_\varrho - 1)} \times \right. \\ & \left. \left(\frac{\beta_\varrho q_\varrho}{p_\varrho} \dot{\varrho}^{2 - p_\varrho/q_\varrho} + \mathcal{K} \mathrm{sign}(\mathcal{S}_\varrho) \right) \right]. \end{aligned} \tag{27}$$

Since (27) can be written as

$$\dot{\mathcal{V}}_\varrho = -\mathcal{S}_\varrho \left[\frac{p_\varrho}{\beta_\varrho q_\varrho} \dot{\varrho}^{(p_\varrho/q_\varrho - 1)} \mathcal{K} \mathrm{sign}(\mathcal{S}_\varrho) \right] \tag{28}$$

$$\leq -\frac{\mathcal{K} p_\varrho}{\beta_\varrho q_\varrho} \dot{\varrho}^{(p_\varrho/q_\varrho - 1)} \left| \mathcal{S}_\varrho \right|, \tag{29}$$

it follows that $\dot{\mathcal{V}}_\varrho < 0$ for all $\varrho \neq 0$. Let us now define

$$\rho(\varrho) := \frac{\mathcal{K}}{\beta_\varrho} \frac{p_\varrho}{q_\varrho} \dot{\varrho}^{(p_\varrho/q_\varrho - 1)}, \tag{30}$$

then $\dot{\mathcal{V}}_\varrho$ can be expressed as

$$\dot{\mathcal{V}}_\varrho = \rho(\varrho) \left| \mathcal{S}_\varrho \right| \tag{31}$$

As $\rho(\varrho) > 0 \; \forall \; \dot{\varrho} \neq 0$, the Lyapunov stability criteria is satisfied for all $\dot{\varrho} \neq 0$. Thus, the errors ϱ and $\dot{\varrho}$ will subsequently vanish after $\mathcal{S}_\varrho = 0$. On substituting the expression for δ using (25) in (20), we obtain

$$\begin{aligned} \ddot{\varrho} = & -2\xi\omega_n \dot{a_m} - a_m \omega_n^2 - \ddot{a}_m^c + \omega_n^2 \left[-\frac{1}{\omega_n^2} \left\{ -2\xi\omega_n \dot{a}_m \right. \right. \\ & \left. \left. - a_m \omega_n^2 - \ddot{a}_m^c + \beta_\varrho \frac{p_\varrho}{q_\varrho} \dot{\varrho}^{2 - p_\varrho/q_\varrho} + \mathcal{K} \mathrm{sign}(\mathcal{S}_\varrho) \right\} \right], \end{aligned} \tag{32}$$

which is simplified to

$$\ddot{\varrho} = -\beta_\varrho \frac{p_\varrho}{q_\varrho} \dot{\varrho}^{2 - p_\varrho/q_\varrho} - \mathcal{K} \mathrm{sign}(\mathcal{S}_\varrho). \tag{33}$$

It readily follows that for $\dot{\varrho} = 0$, the expression in (33) reduces to

$$\ddot{\varrho} = -\mathcal{K} \mathrm{sign}(\mathcal{S}_\varrho). \tag{34}$$

Observe from (34) that if $\mathcal{S}_\varrho > 0$, then $\ddot{\varrho} < -\mathcal{K}$ and if $\mathcal{S}_\varrho > 0$, we have $\ddot{\varrho} > \mathcal{K}$. This essentially means that $\dot{\varrho} = 0$ is not an attractor and there exist a small neighbourhood, $\mathcal{N}(\zeta) : |\varrho| < \zeta \; \forall \; \zeta > 0$. Therefore, the trajectories will cross the boundaries $\dot{\varrho} = \zeta$ and $\dot{\varrho} = -\zeta$ in a finite time irrespective of their initial values and are always attracted toward the sliding manifold, (21) in finite time. During sliding mode, we have

$$\dot{\varrho} = -\beta_\varrho d^{q_\varrho / p_\varrho}. \tag{35}$$

If we solve for a time t_2 such that $\varrho = 0 \; \forall \; t > t_2$ for a given initial condition $\varrho(t_0)$ at $t = t_0$, then we obtain t_2 as

$$t_2 = t_0 - \frac{1}{\beta_\varrho} \int_{\varrho(t_0)}^{0} \varrho^{-q_\varrho/p_\varrho} \, \mathrm{d}(\varrho),$$
$$= t_0 + \frac{p_\varrho}{\beta_\varrho (p_\varrho - q_\varrho)} \varrho^{\frac{p_\varrho - q_\varrho}{p_d}} \varrho(t_0). \tag{36}$$

As $(p_\varrho - q_\varrho)$ positive even integer, ϱ converges to zero in a finite time, t_2, and remains on it for all future times. Furthermore, $\dot{\varrho} = 0$ within the same time interval, implying that, $a_m^c \to a_m$.

5. SIMULATION STUDIES

In this section, we show the efficacy of the proposed separate guidance and control path-following feedback controller with two different geometrical paths: a straight line and an orbital path. For simulations, we choose the value of ω_n and ξ as 30 rad/s and 0.5, respectively, for each case. Table 1 presents the rest of the controller parameters used in the simulations. We choose the UAV's speed as 10 m/s. To demonstrate the robustness of the proposed separate guidance and control algorithm, we consider a continuous time-varying disturbance as $0.1\sin(t)$, which emulates the effect of wind gusts and other imperfections either not considered or neglected in the control design.

Table 1. Simulation Parameters.

Parameters	η	β_d	p_d	q_d	$\mathcal{K}$	β_ϱ	p_ϱ	q_ϱ
Values	30	1	15	13	1000	90	15	13

5.1 Straight-line Path

In this subsection, we consider that the UAV follows a straight line path depicted in Fig. 2(a). The Cartesian coordinates for p_1 and p_2 are assumed to be given by $(10\text{m}, 10\text{m})$ and $(155\text{m}, 155\text{m})$, respectively. To validate the efficacy of the proposed design, we have considered several initial conditions in the simulations, but we are presenting only two distinct scenarios to show the legibility of the results. In the first scenario, the UAV's initial position is considered at $(10\text{m}, 20\text{m})$, while in the second, it starts at $(10\text{m}, 0\text{m})$.

We demonstrate the performance of the UAV under the derived guidance command (12) and (25) through Fig. 4. Fig. 4(a) depicts that the proposed separate guidance and control feedback controller is able to drive the sliding surface to zero within a finite time soon after the steering angle error converges to zero. This further leads to the term appearing in the denominator of (12), $\cos(\psi - \psi_d)$, to become unity as $\psi = \psi_d$. The perpendicular distance and corresponding velocity between the UAV and the desired path converge to zero during the same time interval, as depicted in Fig. 4(b). Note that these variables are driven to zero from any arbitrary initial conditions ensuring the global convergence of the proposed controller. Figure 4(c) illustrates the commanded and the achieved lateral accelerations. The achieved lateral acceleration is required to steer the UAV on the desired straight-line path and maintain it there for all future times. It is evident that the control effort requirement is reasonable during the transient phase when the sliding mode has not yet

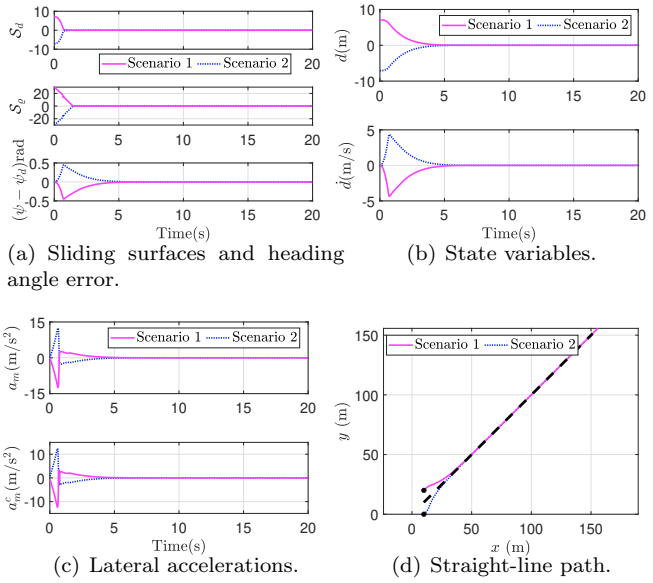

(a) Sliding surfaces and heading angle error. (b) State variables. (c) Lateral accelerations. (d) Straight-line path.

Fig. 4. UAV following a straight-line path for various initial conditions.

occurred. However, once the position and velocity errors vanish, the lateral acceleration demands are ideally zero. Such a feature is always desirable, and it evidences that the proposed controller reduces UAV's maneuverability requirement as soon as the sliding mode is enforced. Note that with suitable controller parameters, one can alter the reaching and sliding phases depending on the actuator's physical limits. Figure 4(d) portrays the UAV's trajectories for both of the scenarios, demonstrating the global convergence to the path.

5.2 Orbital Path

We now consider a circular orbit of a radius of 20m which the UAV is required to follow. Similar to the previous case, we consider two different simulation scenarios. In the first scenario, the UAV is initially located inside the circular orbit, and its initial position is $(-20\text{m}, 10\text{m})$. On the other hand, in the second scenario, it is located at $(-20\text{m}, 25\text{m})$, which is outside the circular orbit. It is evident from Fig. 5, that the sliding manifold and error profiles exhibit a similar profile as in the earlier scenario. This is because the proposed feedback controller is independent of the path curvature information, unlike several other existing approaches that were developed for specific paths. One may also notice that, in both scenarios, the UAV starts to follow the desired path in almost the same amount of time regardless of the initial distance from the path, ensuring lesser maneuverability demands for the UAV.

6. CONCLUSIONS

In this paper, we proposed a robust feedback design for the guidance and the control subsystems for a UAV to follow the desired path in the absence of path curvature information. This makes the approach more suitable for practical implementation and allows a more general treatment of the path-following problem. The proposed controller guarantees that the UAV tracks its desired path within a finite time. We have also shown that nullifying the

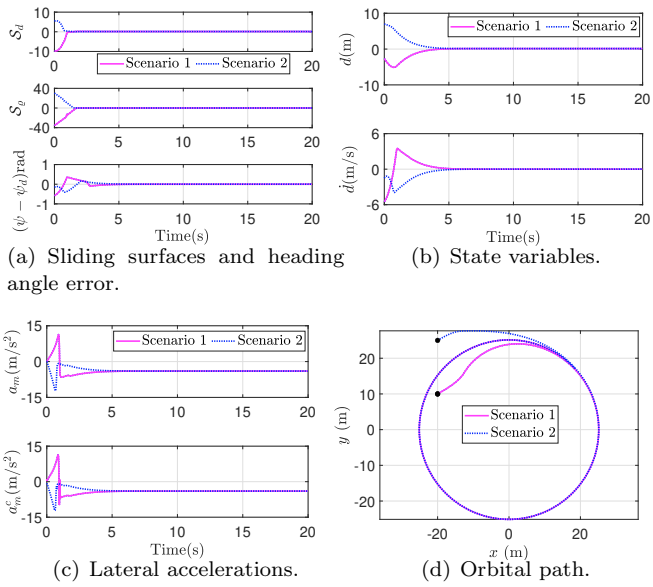

(a) Sliding surfaces and heading angle error.
(b) State variables.
(c) Lateral accelerations.
(d) Orbital path.

Fig. 5. UAV following an orbital path starting from various initial conditions.

perpendicular distance between the UAV and its desired path is sufficient for the UAV to track its desired path, leading to global convergence to the path. Validations of the proposed strategy under various scenarios attested to the robust performance on benchmark path constructs, namely a straight-line path and a circular orbit, with different initial configurations. We also observed the UAV's maneuverability requirements reduced in the sliding phase, which is highly desirable in practical scenarios. The performance of the proposed controller in the presence of external disturbances further strengthens the merits of the proposed design. Incorporating UAV dynamics and obstacle-avoidance algorithms into the design could be an interesting direction for future work.

7. ACKNOWLEDGEMENTS

This work was supported in part by the Centre of Propulsion Technology (CoPT), Defence Research and Development Organisation, India [Grant No. I-F-1-1 (RD/0120-COPTG00-001)].

REFERENCES

Cabecinhas, D., Silvestre, C., Rosa, P., and Cunha, R. (2007). Path-following control for coordinated turn aircraft maneuvers. In *AIAA Guidance, Navigation, and Control Conference and Exhibit*, 1–19. AIAA 2007-6656.

Frew, E.W., Lawrence, D.A., Dixon, C., Elston, J., and Pisano, W.J. (2007). Lyapunov guidance vector fields for unmanned aircraft applications. In *American Control Conference*, 371–376.

Gates, D.J. (2010). Nonlinear path following method. *Journal of Guidance, Control, and Dynamics*, 33(2), 321–332.

Gurfil, P. (2003). Zero-miss-distance guidance law based on line-of-sight rate measurement only. *Control Engineering Practice*, 11(7), 819–832.

Gutman, S. (2008). Can lead-lag guidance compensator guarantee zero-miss-distance? *Journal of Guidance, Control, and Dynamics*, 31(3), 779–782.

Kaminer, I., Pascoal, A., Xargay, E., Hovakimyan, N., Cao, C., and Dobrokhodov, V. (2010). Path following for small unmanned aerial vehicles using l1 adaptive augmentation of commercial autopilots. *Journal of Guidance, Control, and Dynamics*, 33(2), 550–564.

Kumar, S. and Kumar, S.R. (2022a). Barrier lyapunov-based nonlinear trajectory following for unmanned aerial vehicles with constrained motion. In *International Conference on Unmanned Aircraft Systems*, 1146–1155.

Kumar, S. and Kumar, S.R. (2022b). Finite-time convergent robust trajectory tracking for unmanned aerial vehicles. In *International Conference on Unmanned Aircraft Systems*, 1166–1175.

Kumar S, N., Nanavati, R.V., and Kumar, S.R. (2022). Robust nonlinear guidance strategies for survival of cooperating unmanned aerial vehicles against pursuing attackers. *Proc. of the IMechE., Part G: Journal of Aerospace Engineering*, 09544100221115238.

Lawrence, D.A., Frew, E.W., and Pisano, W.J. (2008). Lyapunov vector fields for autonomous unmanned aircraft flight control. *Journal of Guidance, Control, and Dynamics*, 31(5), 1220–1229.

Liu, C., McAree, O., and Chen, W.H. (2012). Path-following control for small fixed-wing unmanned aerial vehicles under wind disturbances. *International Journal of Robust and Nonlinear Control*, 23(15), 1682–1698.

Lizarraga, M., Curry, R., and Elkaim, G.H. (2013). Flight test results for an improved line of sight guidance law for uavs. In *American Control Conference*, 818–823.

Nelson, D.R., Barber, D.B., McLain, T.W., and Beard, R.W. (2007). Vector field path following for miniature air vehicles. *IEEE Transactions on Robotics*, 23(3), 519–529.

Park, S., Deyst, J., and How, J.P. (2007). Performance and lyapunov stability of a nonlinear path following guidance method. *Journal of Guidance, Control, and Dynamics*, 30(6), 1718–1728.

Ratnoo, A., Hayoun, S.Y., Granot, A., and Shima, T. (2015). Path following using trajectory shaping guidance. *Journal of Guidance, Control, and Dynamics*, 38(1), 106–116.

Ratnoo, A., Sujit, P., and Kothari, M. (2011). Adaptive optimal path following for high wind flights. *IFAC Proceedings Volumes*, 44(1), 12985–12990.

Rhee, I., Park, S., and Ryoo, C.K. (2010). A tight path following algorithm of an uas based on pid control. In *Proceedings of SICE Annual Conference*, 1270–1273.

Singh, S.K., Sinha, A., and Kumar, S.R. (2022). Nonlinear control design for an unmanned aerial vehicle for path following. *IFAC-PapersOnLine*, 55(1), 592–597.

Sinha, A., Kumar, S.R., and Mukherjee, D. (2021). Three-dimensional guidance with terminal time constraints for wide launch envelops. *Journal of Guidance, Control, and Dynamics*, 44(2), 343–359.

Yamasaki, T., Balakrishnan, S.N., and Takano, H. (2013). Separate-channel integrated guidance and autopilot for automatic path-following. *Journal of Guidance, Control, and Dynamics*, 36(1), 25–34.

Yoshitani, N. (2010). Flight trajectory control based on required acceleration for fixed-wing aircraft. In *Proceedings of the 27th International Congress of the Aeronautical Sciences*, 1–10.